forests

Article

The Effect of Green Stormwater Infrastructures on Urban-Tier Human Thermal Comfort—A Case Study in High-Density Urban Blocks

Haishun Xu *, Jianhua Liao and Yating Hong

The College of Landscape Architecture, Nanjing Forestry University, Nanjing 210037, China
* Correspondence: xuhaishun@njfu.edu.cn

Abstract: Green stormwater infrastructure (GSI) is a key approach to greening and cooling high-density blocks. Previous studies have focused on the impact of a single GSI on thermal comfort on sunny days, ignoring rainwater's role and GSI combinations. Therefore, based on measured data of a real urban area in Nanjing, China, this study utilized 45 single-GSI and combination simulation scenarios, as well as three local climate zone (LCZ) baseline scenarios to compare and analyze three high-density blocks within the city. Among the 32 simulations specifically conducted in LCZ1 and LCZ2, 2 of them were dedicated to baseline scenario simulations, whereas the remaining 30 simulations were evenly distributed across LCZ1 and LCZ2, with 15 simulations allocated to each zone. The physiological equivalent temperature (PET) was calculated using the ENVI-met specification to evaluate outdoor thermal comfort. The objective of this research was to determine the optimal GSI combinations for different LCZs, their impact on pedestrian thermal comfort, GSI response to rainwater, and the effect of GSI on pedestrian recreation areas. Results showed that GSI combinations are crucial for improving thermal comfort in compact high-rise and mid-rise areas, while a single GSI suffices in low-rise areas. In extreme heat, rainfall is vital for GSI's effectiveness, and complex GSI can extend the thermal comfort improvement time following rainfall by more than 1 h. Adding shading and trees to GSI combinations maximizes thermal comfort in potential crowd activity areas, achieving up to 54.23% improvement. Future GSI construction in high-density blocks should focus on different combinations of GSI based on different LCZs, offering insights for GSI planning in Southeast Asia.

Keywords: green stormwater infrastructure; ENVI-met; high-density urban block; thermal comfort; combination scenario simulation

Citation: Xu, H.; Liao, J.; Hong, Y. The Effect of Green Stormwater Infrastructures on Urban-Tier Human Thermal Comfort—A Case Study in High-Density Urban Blocks. *Forests* **2024**, *15*, 862. https://doi.org/10.3390/f15050862

Academic Editor: Elisabetta Salvatori

Received: 24 April 2024
Revised: 10 May 2024
Accepted: 13 May 2024
Published: 15 May 2024

1. Introduction

In the past ten years, the acceleration of urban development and the release of anthropogenic heat have led to an increasing urban heat island effect [1], and this enhanced effect has become an urgent obstacle to sustainable development, affecting the morbidity and mortality caused by heat stress in the surrounding environment [2,3] and the cooling demand of indoor spaces [4,5], as well as the degradation of air quality, deterioration of the water environment, and disturbance of biological habitats [6]. Therefore, by means of forecasting, determining feasible measures in the urban environment to reduce the impact of the UHI can provide a scientific reference for future sustainable urban development and planning.

As representatives of urban areas in developing countries, most urban areas in China have experienced high-density population growth, constructed land expansion, energy pressure, and urban flooding problems caused by subsequent changes. The Sponge City (SC) was launched in 2013 to create a new sponge-like urban water management system, which is similar to the Best Management Practices (BMPs) in the United States [7,8], Water Sensitive Urban Design (WSUD) in Australia [9,10], and the New Zealand government's

Low Impact Urban Design and Development (LIUDD) program [11]. It reduces runoff, peak flow, and pollutant concentrations by improving infiltration, retention, storage, purification, and drainage systems and is more advantageous than traditional drainage. In conclusion, the Sponge City approach represents a promising solution for sustainable urban water management in China and other developing countries.

Common technologies applied in the construction of SCs include green stormwater infrastructure (GSI), which has different types and scales. Implementation forms of GSI at the urban-block scale include roof greening, vertical greening (VG), green spaces, bioretention facilities, and permeable pavement (PP) [5,12]. Because the location of GSI is not limited to the ground, it is more flexible in high-density urban areas. It can reduce urban temperature by increasing the green coverage area of the city, enhancing evapotranspiration [13], alleviating ground temperature increase, increasing building insulation, and improving the cooling efficiency of green spaces [14,15]. Recently, there has been a progressive increase in the number of studies examining the impact of GSI on thermal comfort [16–18], indicating that people are not only concerned about the management of urban water through GSI but also about its impact on the urban thermal environment.

Therefore, this study selected four instances of GSI with different attributes to assess the influences of GSI on the thermal comfort on building façades, building tops, ground, and green spaces. The impact of these GSIs on the thermal environment has been verified in many studies. On building façades, VG can contribute significant environmental, social, and economic benefits to the built environment [19]. Its thermal impact depends on the shading capacity of the selected vegetation, the plant evapotranspiration process, and the substrate [20–22]. Acero showed that the thermal comfort of outdoor spaces near VG can be lower by one category (for example, from hot to warm) [23]. Rooftops account for approximately 20%–25% of the urban area [24]. Studies have shown that green roofs can reduce heat flow through the building by approximately 80% in summer [25] and further improve the cooling effect by increasing irrigation. An [26] experimentally observed that adding an aquifer under the soil matrix of a green roof (GR) to retain rainwater for irrigation resulted in a temperature drop of 1.3 °C. However, studies have also shown that its impact on the surrounding environment can only produce a significant temperature reduction at the roof level. In addition, the cooling effect of rain gardens (RGs), a special form of green space that retains rainwater through lower planes and permeable structures, has been verified in several studies [27]. Previous studies have focused mostly on the plant species composition, species characteristics [28], and rainwater infiltration efficiency [29–32] of RGs. Finally, surface heating can be alleviated by special ground materials [33–35], such as materials or coatings with high reflectivity, which can reduce the surface temperature [36] to obtain a so-called cold surface. Moreover, some ground materials can retain a portion of the rainwater after a rain by increasing the porosity of the surface, thereby delaying ground heating [37]. This (PP) is often used as a source collection measure in SCP (Sponge City Plan) [12].

Although these studies have considered the applicability of single GSI in response to climate change and urbanization, there are few studies on GSI combinations, and rainwater has not been considered as a specific factor affecting urban thermal comfort in extreme heatwave weather. Despite the proposal that the cooling efficiency of the combination of green walls (GWs) and GRs is higher than that of the two separate forms of GSI [38], few studies have assessed the extent of the efficiency improvement and the performance of combinations of three or even four instances of GSI.

This study innovatively explored the potential of different forms of GSI and their combinations to improve the thermal comfort of the pedestrian level before, during, and after rain in afternoon heavy-rain weather under a heat wave. An urban block located in the center of Nanjing, China, was selected, and an ENVI-met model of high-density blocks was constructed with meteorological data measured in situ by meteorological stations and sites as the model boundary data.

Since this article focuses on urban high-density neighborhoods, the concept of Local Climate Zone (LCZ) systems is introduced in the selection of study areas. An LCZ is an objective, universal, and standardized method for classifying local thermal climate for urban temperature research. In this article, urban high-density neighborhoods are interpreted as urban areas that meet the LCZs1–3 standards. There are differences in heat island intensity between different LCZ plots and between plots of the same type of LCZ. Among them, the heat island intensity of compact building areas (LCZ1, 2, and 3) tends to be the highest, followed by open building areas (LCZ4, 5) and large low-rise building areas (LCZ8) [39]. This study mainly focuses on common high-density neighborhoods in the city center, namely LCZs1–3 in the LCZ classification, which have high-density building clusters and a high rate of greening, making them key areas where urban heat islands pose a threat to the population.

The purposes of this study were to determine (1) the optimal combination of GSI for different local climate zones (LCZs) and their combined effects on pedestrian-level thermal comfort, (2) the degree of response of different GSI facilities to rainwater, and (3) the impact of GSI construction on major pedestrian recreation areas. To compare the efficiency of thermal comfort improvement, a new physiological equivalent temperature (PET)-derived index (%DPET) [40] was introduced. It was used to compare the improvement efficiency of different programs. These findings help to inform potential actions taken by policymakers, managers, and designers to improve the welfare provisioning and perception of GSI in high-density urban neighborhoods and to improve the social well-being and quality of life of urban communities.

2. Materials and Methods

2.1. Research Framework

Figure 1 illustrates the comprehensive evaluation process of the thermal comfort of the four GSI strategies and their 15 combinations used in this study in combination with the three LCZs. The process includes four parts, namely field measurement and weather station data collection; model verification and experimental material parameter setting; 48 scenario simulations, including three baseline scenarios; and thermal comfort evaluation index setting based on PET. Finally, based on the research results, the ability of the GSI combinations in the different scenarios to increase thermal comfort efficiency was evaluated.

2.2. Study Area and Data Collection

China's Yangtze River Delta region includes a typical high-density urban building agglomeration, within which Nanjing is known as the 'stove' because of its common high-temperature weather in summer. In the past 20 years, the area of heat island and strong heat island in Nanjing increased rapidly from 6.48% to 40.81%. Land surface temperature showed a significant urban–rural gradient difference. The range of the strong heat island coincided with the center of gravity of the city and expanded with the expansion of the built-up area [41].

Nanjing, situated in the eastern part of China, experiences a northern subtropical monsoon climate that is distinguished by abundant rainfall and four distinct seasons. Notably, due to the significant urban heat island (UHI) effect and persistent heat waves during the summer months, the city is often referred to as a "furnace city". According to Nanjing's climatological normal (1991–2020), the summer months, in particular, experience frequent rainfall and high temperatures, which are conducive to studying the impact of various strategies, such as low-impact development (LID), on stormwater management and microclimate improvement [42]. Furthermore, the Koppen Geiger Climate Classification designates Nanjing's climate as closer to the subtropical humid climate (Cfa), which aids in explaining the city's prevalent high-temperature weather in summer and its associated heat island effect.

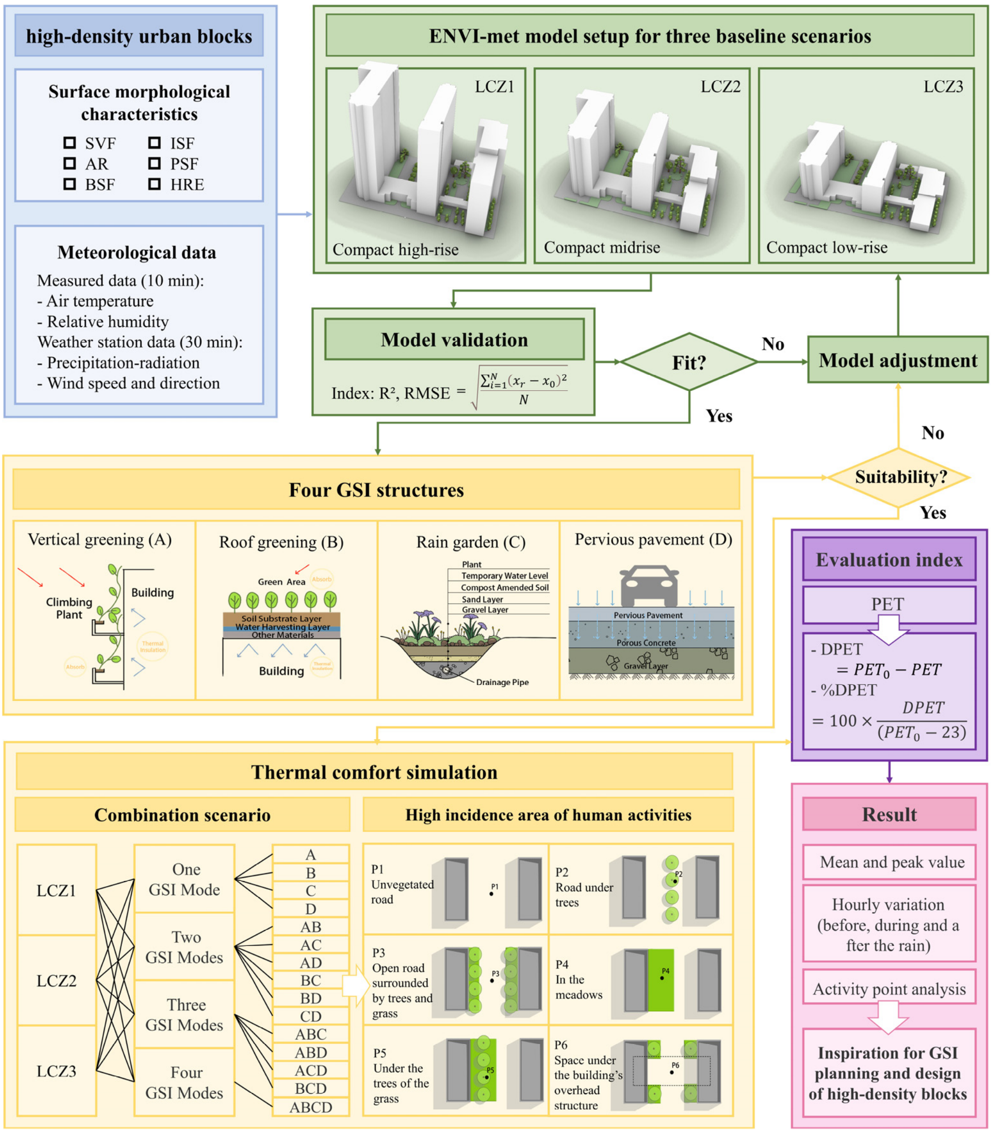

Figure 1. Research framework. Sky-view factor (SVF): the ratio of the number of sky hemispheres visible from the ground to the number of accessible hemispheres; aspect ratio (AR): average height-to-width ratio of street canyons (LCZs1–7), building spacing (LCZs8–10), and tree spacing (LCZsA–G); building surface fraction (BSF): ratio of floor area to total floor area (%); impervious surface fraction (ISF): ratio of impervious surface area (pavement and rock) to total surface area (%); pervious surface fraction (PSF): ratio of permeable surface area (bare soil, vegetation, and water) to total surface area (%); height of roughness elements (HRE): geometric mean of building height (LCZs1–10) and tree/plant height (LCZs A–F) (m).

To examine the alleviation of the impact of the heat island effect of urban high-density blocks during heat wave, a city center with a strong heat island was selected as the research area, as depicted in Figure 2. Most of the urban areas with the highest temperature are one of three types of compact LCZ, namely LCZ1, the compact high-rise type; LCZ2, the compact middle–high type; and LCZ3, the compact low-rise type. These LCZs typically have a high building density and a lack of ground greening. According to the surface morphological characteristic parameters of LCZs, the research area consists of LCZ2. To promote research results that cover most of the high-density neighborhoods in the city center to the greatest extent possible, this study modified the surface morphological characteristic parameters on the basis of the measured parameters and extended the original site to LCZ1 and LCZ3 types, which has been proven feasible in many studies [43].

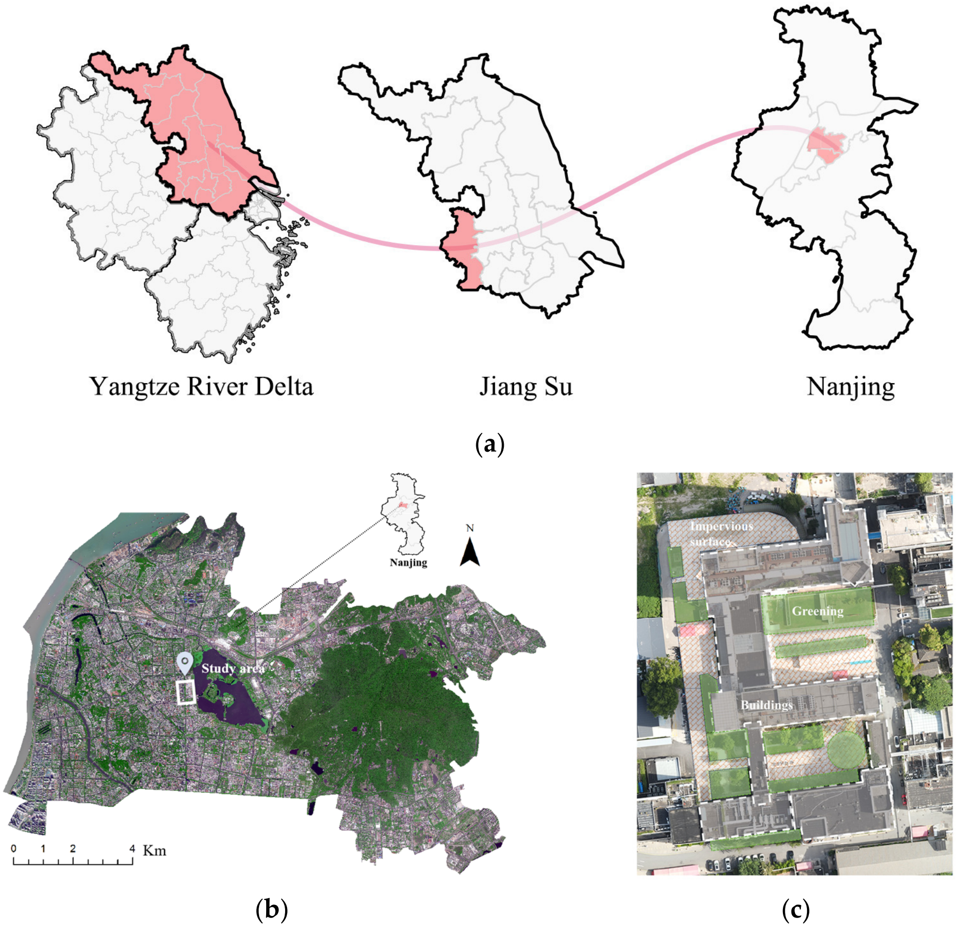

Figure 2. (**a**) The location of Nanjing in the Yangtze River Delta region; (**b**) the location of the study area in the center of Nanjing; (**c**) UAV aerial images of the study area.

As a research area, Jiangsu Cancer Hospital can acquire continuous temperature and humidity information during summer by placing temperature and humidity meters at the location. Table 1 shows a comparison between the standard statistical data of the local climatic zone and the geometric and surface coverage characteristics of the study case, as well as the model parameters of LCZ1 and LCZ3 as extended based on the measured data. The survey area was a rectangle of 139 m × 78 m (10,842 m^2).

Table 1. Differences between the study cases and the LCZ classification criteria. SVF: sky-view factor; AR: aspect ratio; BSF: building surface fraction; ISF: impervious surface fraction; PSF: pervious surface fraction; HRE: height of roughness elements.

Study Case	SVF		AR		BSF		ISF		PSF		HRE	
	Standard	Case	Standard	Case	Standard	Case	Standard	Case	Standard	Case	Standard	Case
LCZ1 Compact high-rise	0.2–0.4	0.34	>2	2.27	40–60	47.2	40–60	42.6	<10	10.2	>25	60.5
LCZ2 Compact midrise	0.3–0.6	0.43	>0.75–2	1.47	40–70	48.9	30–50	35	<20	17.6	10–25	25.2
LCZ3 Compact low-rise	>0.7	0.90	0.75–1.5	0.96	40–70	47.2	20–50	29.7	<30	23.1	3–10	8

2.3. Meteorological Data Record

A temperature and humidity sensor (NB/LoRa; JXCT Electronics Co., Ltd., Weihai, China) was selected to conduct an actual survey of the study area and record relevant data. In summer, from 00:00 13 August to 16:00 23 August 2022, continuous observation was conducted for 10 days under various weather conditions. The data sampling interval was 10 min. The temperature measurement range of the measuring instrument was −40%~80 °C, with a measurement accuracy of ±0.2 °C and a resolution of 0.1 °C. The humidity measurement range was 0%~100%RH, with a measurement accuracy of ±3% RH and a resolution of 0.1%RH. The temperature was measured at a distance of 1.5 m from the ground, and the measurement was continuously fixed.

The analysis to evaluate the effects of various urban features on microclimate was based on simulations of the urban microclimate using ENVI-met software (v 5.5.1, ENVI-met, GmbH, Essen, Germany), a computational fluid dynamics software that has been used and tested widely [44–53], especially in Asia [53,54]. Studies have shown that, for the ENVI-met model setting, the model provides the best performance by fully forcing meteorological boundary conditions and localizing the material. Therefore, both the meteorological boundary conditions and materials need to be localized [54]. Hence, this study collected meteorological information by field measurement to ensure the accuracy of the model. The simulation was performed using the latest release (v 5.5.1). The program includes a Bio-Met submodule for calculating the PET index and a fully forced meteorological module for rain. As previously mentioned, this study aimed to promote the impact of different GSI combinations on pedestrian-level thermal comfort in a rainwater environment; thus, the daily data of 18 August (rainy day) were used as the input values of temperature and humidity. Other meteorological data were provided by the Nanjing Meteorological Station.

2.4. ENVI-Met Parameter Settings and City-Specific Models for the Case Study

The simulated area for the modeling of the study area (LCZ2) in ENVI-met was 88 m × 141 m × 75 m. Considering the building height and the use requirements of the ENVI-met model, a 100 m buffer was set around the simulated area using loam soil, and a 100 m buffer was set at the top according to the highest building height. This was done to solve the problem that the model does not work reliably near the boundary. The resolution of the horizontal grid of the model was 1 m × 1 m × 5 m, the accuracy of the vertical grid was reduced to improve the simulation efficiency, and the lowest grid near the ground was split into five cells, allowing the part near the surface to have accurate output. Temperature and humidity data measured in the field every half hour and wind speed, wind direction, radiation, precipitation, and other conditions obtained from the Nanjing meteorological station were used as the transverse boundary conditions. The measurement height for temperature and relative humidity was 1.5 m, and the measurement height of wind speed and wind direction was 10 m. The initialization time of the ENVI-met simulation was set as 6:00 a.m. Eastern 8 time zone on 18 August 2022, and the total simulation time was 14 h. The roughness coefficient around the simulated area was assumed to be a typical value of 0.1 for urban medium-density areas.

The sensitivity of the measured and simulated data was analyzed using correlation and difference measures. The R^2 value was used to quantify the correlation between the simulated and observed values, and the RMSE was used to assess the error between the two metrics.

Simulation errors have been reported previously [55–58] due to the use of simple forcing of meteorological boundary conditions, the uncertainty introduced into the model by keeping a single wind direction, and the fact that anthropogenic energy release cannot be considered, which can result in significant underestimation of temperature and humidity. The verification results of this study showed that the R^2 of the overall average temperature of the site was 0.997 and that the RMSE was 0.034. The R^2 of the overall average humidity of the site was 0.996, and the RMSE was 12.627. These results indicate that the average simulation data were highly similar to the measured data. Thus, the ENVI-met simulation did provide acceptable accuracy for the outdoor-environment simulation of this study. Table 2 shows the setting parameters of the four GSIs in ENVI-met.

Table 2. GSI simulation parameters.

Vertical greening (A)	Albedo	0.2
	Emissivity	0.97
	Greening rate (%)	100
	Leaf area index (m^2/m^2)	3
	Leaf angle distribution	0.5
	Plant thickness (cm)	30
	Aquifer thickness (cm)	5
Roof greening (B)	Albedo	0.2
	Emissivity	0.97
	Greening rate (%)	100%
	Leaf area index (m^2/m^2)	3
	Leaf angle distribution	0.5
	Plant thickness (cm)	20
Rain garden (C)	Albedo	0.2
	Emissivity	0.97
	Soil materials	Silty clay loam
	Plant variety	Zoysia japonica
	Height of plant (cm)	20
	Saturated water thickness (cm)	20
Pervious pavement (D)	Albedo	0.40
	Emissivity	0.9
	Material	Pervious cement

2.5. PET and Suggested PET Index

We used DPET and %DPET to determine thermal comfort. PET is defined as the air temperature in a typical indoor setting (without wind and solar radiation) at which the heat budget of the human body is balanced with the same core and skin temperature as under the complex outdoor conditions being assessed. Using ENVI-met, the PET index was calculated according to the reduced form of the Munich Energy-balance Model (MEMI) proposed by Höppe [59], which was modified by Walther and Goestchel [60]. Related studies have been conducted in some areas of Nanjing to quantify the thermal comfort using PET.

To compare the effectiveness of different mitigation options for improving thermal comfort more precisely, two indicators previously studied by Schibuola [40] were used to highlight the absolute and relative advantages of applying a solution over the reference scenario. Index (1) determines the difference between the PET value and the initial PET (PET_0) to obtain the corresponding final PET.

$$DPET = PET_0 - PET \tag{1}$$

DPET indicates the strength of the mitigation protocol in reducing PET but is not directly related to improvement in comfort. Therefore, in Equation (2), a further exponential %DPET is recommended to represent the effectiveness of comfort.

$$\%DPET = 100 \times \frac{DPET}{(PET_0 - 23)} \tag{2}$$

%DPET is the ratio between the reduction in PET after the application of mitigation measures and the PET value outside the comfort range (23 °C), indicating the efficiency of different mitigation measures in improving thermal comfort.

3. Results

3.1. Mean and Peak Values of Regional DPET and %DPET

Figure 3 clearly shows the differences in outdoor thermal comfort among 45 simulation scenarios in LCZ1, 2, and 3. Generally, LCZ1 and LCZ2 need complex GSI combinations to make up for a lack of ground vegetation and too much impervious surface area. LCZ3, however, has fewer buildings, allowing GSI-induced cold air to disperse more easily. Therefore, GSI tends to be most effective in LCZ3.

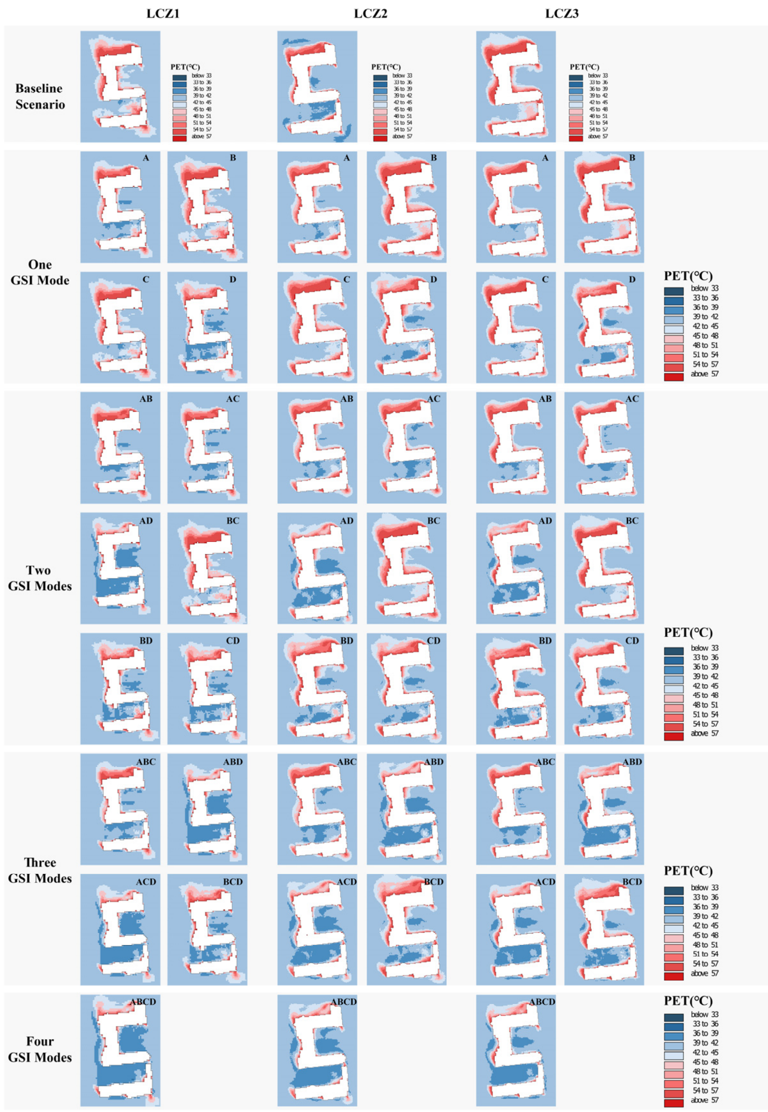

Figure 3. The 48 simulated PET scenarios 2 h after rain (18:00). PET: Physiologically Equivalent Temperature.

The mean and peak values of DPET and %DPET for the different LCZs are presented in Figure 4. Almost every mitigation protocol demonstrated the ability to alleviate the thermal environment, with peak values of DPET and %DPET significantly higher than the corresponding average values. This is the case because building shadows prevent the internal GSI from playing a role, and the increase in green coverage area at the site can improve the thermal comfort effect of GSI. LCZ2 has taller buildings and more impervious surface area. Therefore, among these schemes, LCZ3 exhibited the most favorable overall effect, and LCZ2 had the least desirable effect.

Figure 4a illustrates the effect on PET of applying different GSI combinations to LCZ1. It is evident that GR has a minimal improvement effect in high-rise building areas; however, VG and PP are more suitable mitigation strategies when considered individually. The best GSI combination to improve thermal comfort was ACD, which resulted in a peak %DPET value of 23.81% and a mean value of 8.62%. Figure 4b shows the PET change effect obtained by employing various combinations of GSI measures within LCZ2.

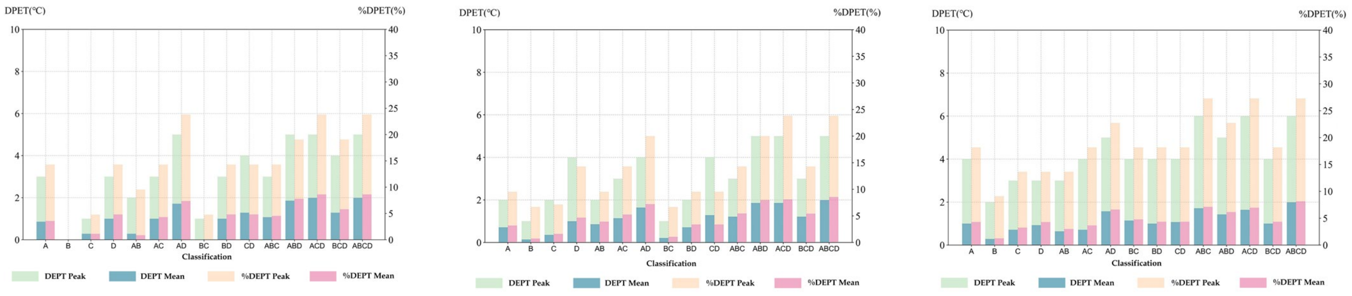

(**a**) (**b**) (**c**)

Figure 4. Mean and peak values of PET and %DPET for (**a**) LCZ1, (**b**) LCZ2, and (**c**) LCZ3.

The reduction in building height enhanced the mitigating role of GR, while RGs became more effective in achieving a positive impact with increased green land rates. Among the mitigation measures, PP stood out, achieving a peak %DPET reduction of 14.29%. The most effective combination was ABCD, reducing DPET by an average of 2 °C and up to 5 °C, corresponding to %DPET reductions of 8.56% and 23.81%, respectively.

Overall, LCZ2 showed more stable but less powerful mitigation effects compared to LCZ1. It is clear that lower buildings and more greenery enhance the effects of GR and RGs. In LCZ3, the peak mitigation of RGs was similar to that of PP, but the average effect was weaker. VG was the best measure, matching the impact of BC, BD, CD, and BCD combinations without VG. For multi-measure combinations, adding GR provided better results than adding PP.

The effect of increasing the complexity of the GSI combination on the improvement of overall thermal comfort was also assessed. According to the simulation experiment, the double GSI model is more unstable. In LCZ1, the double GSI combination lacked a significant strengthening effect, while in LCZ2, efficiency mostly declined. LCZ3 showed better performance, with measure increments yielding over 4% efficiency gains. The three-GSI mode produced the most significant improvement, along with efficiency gains for most combinations. LCZ2 achieved the best performance, averaging a 6.5% increase. In the four-GSI mode, enhancing GR and RG barely improved thermal comfort, while VR and PP increments in LCZ2 had similar effects. PP excelled in LCZ1, while VR excelled in LCZ3. Overall, LCZ2 and LCZ1 favored complex GSI combinations, while LCZ3 benefited more from a single GSI. Among the four forms of GSI, VG increments consistently spurred efficiency growth, regardless of the combination.

In general, more densely built areas with a higher proportion of impervious water require a more complex GSI composition.

3.2. Influence of Rainfall on GSI Combination

Overall, during the high-temperature heat wave, the improvement effect of GSI on the thermal comfort of the outdoor environment was almost zero under the condition of no rain. The improvement effect of almost all forms of GSI peaked 2 h after the rain, and the effect returned to the condition of no rain about 4 h after rain. Among the three LCZs, almost all GSI combinations of LCZ3, as well as the single-GSI mode, could achieve significant efficiency improvement after rain. Among the three or more GSI modes of LCZ2, DPET had the highest value and was the most stable. For LCZ1, the value of DPET was the highest for two or more GSI modes, but the overall trend was unstable, especially in the combinations of GR. Among the four GSIs, VG and PP had the most obvious response to rainwater, and the combination of these two forms of GSI produced a significant improvement in efficiency after rain (Figure 5).

The DPET curve of the simulated scene before the rain was almost zero. However, with the increase in precipitation, the cooling and humidifying effects of VG and PP were enhanced, and RG exhibited a certain effect. One hour after the rain, the site gradually warmed, but the relative humidity of the air remained high, and plant transpiration weakened; thus, the %DPET values of RG and VG decreased. After 2 h, with a decrease in relative humidity, the transpiration of greening was obvious. The rainwater retained in the permeable ground also ensured long-term evaporation after the rain, thereby releasing latent heat and maintaining a more comfortable thermal environment after the rain.

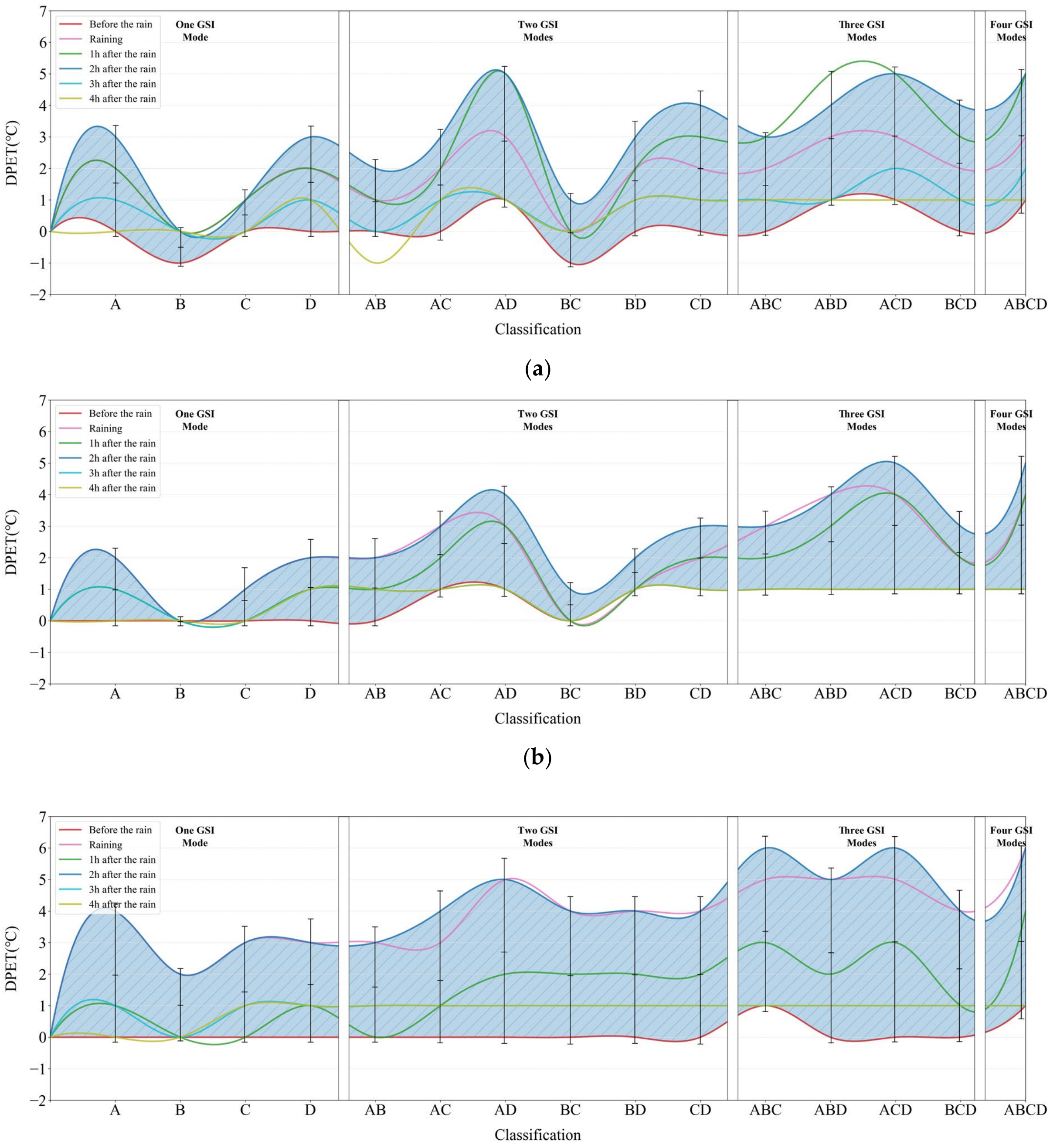

(**a**)

(**b**)

(**c**)

Figure 5. Comparison of DPET values of different GSI combinations before and after rain for (**a**) LCZ1, (**b**) LCZ2, and (**c**) LCZ3.

The combined GSI not only had a higher %DPET in terms of cooling and humidification efficiency but could also generated positive feedback quickly and prolonged the duration of the comfortable thermal environment caused by rainfall. In LCZ1, the four combinations of AD, ABD, ACD, and ABCD had the best cooling and humidifying effects; however, compared with the double GSI mode, the combinations of three and four GSI modes achieved better cooling and humidifying effects 1 h after rain.

In summary, complex GSI combinations can have a faster effect after rain and prolong the time of cooling and humidification after rain. At the same time, rainfall has the most obvious effect on the two GSI modes of VG and PP.

3.3. Cooling and Humidifying Effects of GSI Combinations in Potential High-Risk Areas of Human Activity

To study the effects of different GSI combinations on outdoor populations, the DPET and %DPET values obtained using different GSI combinations were compared in six potential high-risk areas of human activity in the study area (Figure 6). The results showed that it is difficult to achieve a comfortable human thermal perception level in an active area completely exposed to solar radiation but that increasing shading and trees in the active area can effectively improve the effect of GSI on the thermal environment.

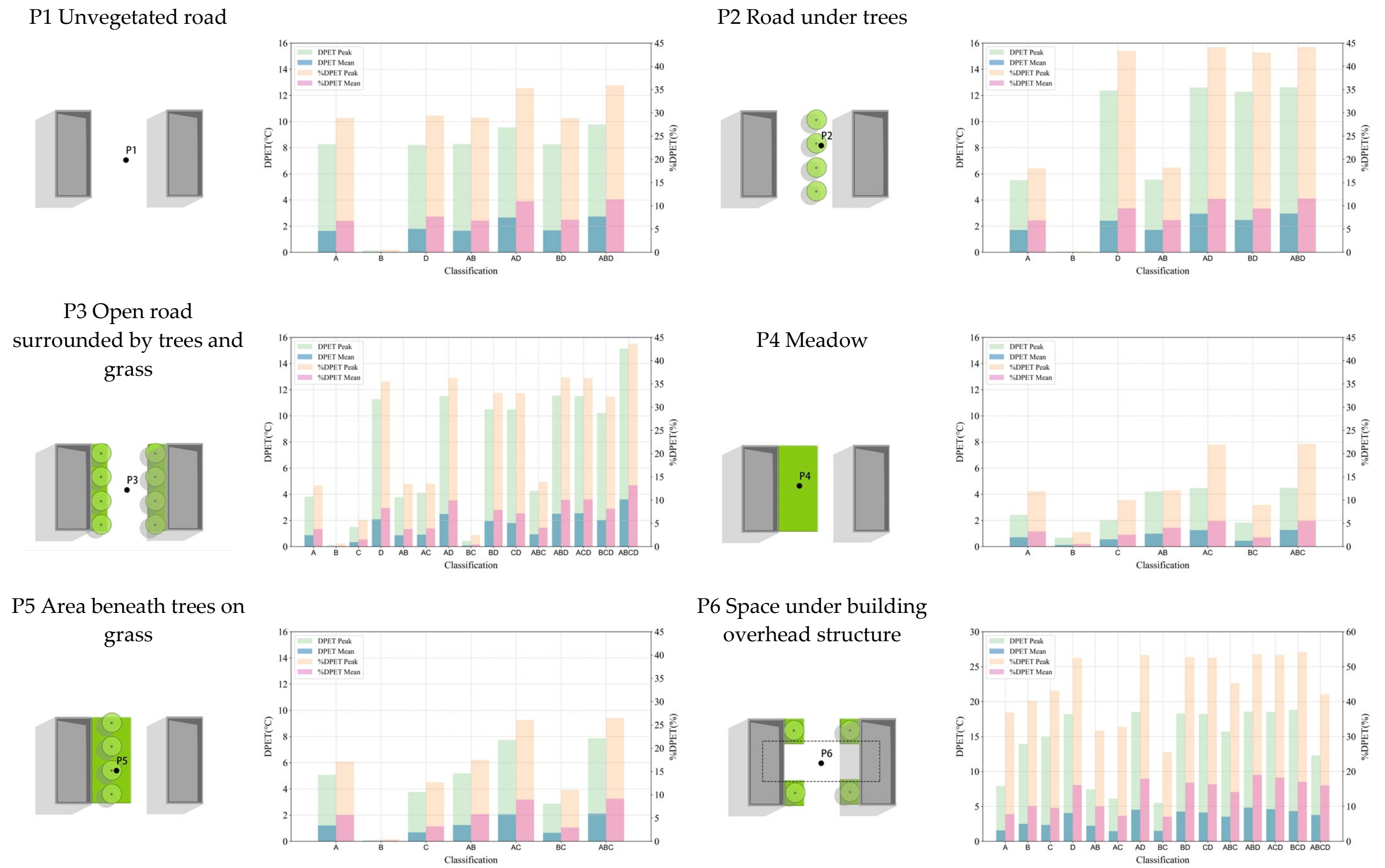

Figure 6. Mean and peak values of DPET and %DPET at various sites.

Among the six observation points, the highest overall temperature occurred on roads without plant coverage, and the most comfortable temperature was on grass covered with trees, indicating that plants have a significant effect in terms of improving the thermal environment during summer. After the addition of GSI, the best comprehensive improvement was observed in P6. For the BCD combination, the peak improvement effect reached 54.23%, indicating that the structure under the building corridor or the gray space of a building are the best places to improve overall thermal comfort when the temperature is high in summer. These are followed by open roads with complete tree coverage and grass structures and roads covered with single trees, both of which had the highest improvement values of between 43% and 45%. The P1 site had the lowest improvement among all sampling sites, followed by lawn space, indicating that bare unvegetated roads and lawn space remain unsuitable for crowd activity, even in urban spaces with mitigation measures.

For all the measurement points on the ground, PP had the most obvious improvement effect in the case of a single GSI, whereas GR and VG on buildings did not have any obvious mitigation effect because of their distance from the sample points. The results of the measurement points on green space showed that the effect of VG is stronger than the effect of RG. With respect to the effect of adding trees, the mitigation efficiency of PP increased by 1.76%, on average, when adding trees at road level and by 13.89% in peak periods. Moreover, according to the comparison between P2 and P3 points, the overall thermal comfort under trees was higher than that of the green periphery with arbor structure. At the green-space level, adding trees on lawns had the most obvious effect on the ABC combination, with an average increase of 3.61% and a maximum increase of 4.42% in %DPET. For the structure under the building corridor, the mitigation effect of PP was stronger than that of RG, followed by GR and VG.

The shading of buildings reduces the evaporation rate of ground water, and the cooling effect after rain lasts for a long time. In addition, it blocks the direct sun at noon, and the cooling effect produced by plant transpiration is obvious. Secondly, verandas were the most efficient locations for GR and VG.

In summary, during high-temperature heat waves in summer, it is necessary to avoid direct exposure to solar radiation in crowded activity venues and appropriately add trees and GSI to outdoor activity venues.

4. Discussion

4.1. Mitigation Effects of Different GSI Combinations on Different LCZs

This study proposed a new framework of GSI settings based on urban high-density neighborhoods and selected three neighborhood models of LCZs to study the impact of 45 GSI combinations on the thermal comfort of the urban population. High-density neighborhoods are common in Southeast Asia and inevitably include too many impervious surfaces and too little ground green space under rapid urban expansion. Therefore, increasing the number of GSI facilities is the primary means of improving thermal comfort in these areas. Many previous studies have considered the improvement of thermal comfort obtained using a single GSI [23,61–67], and some studies have considered the impact of combinations of two forms of GSI [68]. However, few studies have considered combinations of three or four forms of GSI. Nevertheless, in real contexts, especially high-density neighborhoods, GSI usually occurs in the form of combinations [69,70].

The simulation results showed that the GSI combination demand has a significant relationship with the surface morphological characteristics of the study area. Previous studies have reached similar conclusions [71,72]. LCZ2 requires multi-combination GSI the most, followed by LCZ1, and the three-GSI model has obvious efficiency benefits in these two regions. The single-GSI mode has a good effect in terms of improving thermal comfort in LCZ3, and increasing the complexity of GSI cannot greatly improve the thermal comfort of this area.

The best results of the three-GSI mode and the four-GSI mode in LCZ1 and LCZ2 are the same, indicating that setting GR on the roof of high-rise and super high-rise buildings is almost ineffective in terms of improving the overall thermal environment, which is consistent with the results of previous research [73]. Moving from the two-GSI mode to the three-GSI mode results in significantly increased efficiency of the two regions. This occurs because the three-GSI mode ensures at least one ground GSI and one facade GSI, achieving an overall cooling effect of the site without limiting the cooling to locations near the VG [74]. The single-GSI mode of LCZ3 also achieves a better thermal comfort effect because the higher vegetation coverage of LCZ3 leads to a longer cold-air diffusion distance, and the height and floor area of LCZ3 buildings are lower, which results in a lower blocking effect of the horizontal and vertical airflow of the cold air generated by VG and GR [75]. Therefore, LCZ3 does not show a very strong increase in cooling efficiency with higher complexity of GSI, but increasing the complexity of GSI can further increase the thermal comfort of the site.

The comparison of the four types of GSI showed that VG has the best effect in terms of improving the thermal comfort of the site, followed by PP, and that the combination of these two forms of GSI is often the premise for achieving the highest %DPET, which is consistent with the conclusion of previous studies [75]. For instance, as depicted in Figure 4a, the optimal GSI combination to augment thermal comfort was ACD, yielding a peak %DPET value of 23.81% and an average value of 8.62%. VG and PP performed better in LCZ1 than in LCZ2, largely because high-rise structures shield against solar radiation and, thus, slow the surface heating of VG and because the larger hard ground area in LCZ1 results in higher use of PP. However, in the real environment, the cooling effect of VG is greatly affected by building height and distance [76], and the properties of PP may vary with the material accumulated in the internal pores such that it can lose its water retention ability due to blockage [77]. Therefore, when using these two materials, we should consider their service life and use cost.

In short, for developing countries, it is necessary to combine urban construction with ecological planning, urban heat island and urban stormwater management, and water resource planning and to study and formulate GSI construction systems appropriate for different LCZs to ensure that GSI rainwater management and cooling and humidification work together to the greatest extent possible.

4.2. Role of Rainwater in Mitigation Measures

In many countries in Southeast Asia, such as Thailand, Vietnam, and South Korea, high temperatures in summer are often accompanied by rainy weather [50]. Previous studies comparing pre-rain and post-rain conditions have mostly discussed the impact of rainwater on RG and only rarely discussed the relationship between GSI facilities and rainwater. The experiment reported in this study proved that it is difficult for all mitigation measures to improve the thermal comfort of the outdoor environment under the condition of high temperature and no rainfall. However, after rainfall, more complex combinations of GSI led to a longer duration of the mitigation effect, and the mitigation effect peaked 1–2 h after rainfall.

As shown by the peak and average values of %DPET, the mitigation effect of GSI is significantly different before and after rain, and the average value is much lower than the peak value. This occurs because the water stored in the GSI facility evaporates rapidly during extreme heat waves. At the same time, PP and other materials have higher porosity, their transpiration is faster than that of the existing ground, and they are sometimes even more unfavorable than the general infrastructure at improving thermal comfort [78]. When the GSI combination is more complex, the overall cooling effect of the site is more stable, which is conducive to the storage of rainwater, owing to which the cooling duration is longer.

The above situation shows that under the condition of no rain in summer, GSI must be accompanied by artificial rainfall or irrigation to maintain its internal water storage and play its role at the site. At the same time, to slow the temperature increase after rain and prolong the cooling and humidification effects caused by rainfall, the number of GSI types at the site should be increased.

4.3. Influence of GSI Combinations on Outdoor Activity Areas

The cooling and humidifying effects of GSI on a whole block are not sufficient to make all areas suitable for crowd activities; thus, it is very important to perform targeted analyses of the areas where crowds may be active. The results of this study showed that shading and planted trees can improve the cooling and humidifying effects of GSI facilities on the study area.

Among the six sampling points, the most prominent improvement effect occurred at the measuring point under the overhead structure of a building. Under the BCD combination, the peak improvement effect reached 54.23%, which was the closest effect to an comfortable outdoor environment in the study area. At the same time, the overhead structure was also the place where GR and VG had the highest efficiency. This shows that small-scale greening does not significantly improve thermal comfort in summer [79]. In high-density urban neighborhoods, it is only possible to achieve a comfortable outdoor environment under the premise of providing shading in outdoor pedestrian recreation areas, such as by increasing corridors, space under eaves, and building overhead space and appropriately increasing GR and VG in these areas. Among these strategies, on average, the improvement effect of GR was even stronger than that of VG. This may be attributable to the fact that the overall height of the verges in an actual situation is low and GRs are close to the pedestrian level, owing to which the area of VG is reduced, thereby bringing such an improvement effect. This is similar to the conclusion of the study by Gong et al. [12]. Secondly, trees have a significant strengthening effect on the overall improvement effect. When trees were added at road level, the mitigation efficiency of PP increased by 1.76%, on average, and by 13.89% during the peak period. The effect of shadow under trees is significantly stronger than the effect in areas without shadow that are surrounded by trees and grassland.

Therefore, to enhance shading and tree planting in a crowd recreation area, GSI should be placed closer to the crowd to achieve the highest thermal comfort efficiency.

4.4. Limitations of the Study

This study had some inherent limitations. First, the data from this experiment were not long-term, continuous, dynamic data and cannot summarize the overall situation during an entire summer heat wave. In subsequent studies, all rainy days during heat waves can be selected, and their overall patterns can be analyzed.

Second, four kinds of GSI were established to consider only the situation of completely replacing ordinary infrastructure in order to reduce the influence of other factors on the experiment and to simplify the complexity of the experiment. In subsequent studies, based on the actual situation of the building and consideration of the rainwater control rate, a more reasonable GSI ratio and positioning can be established to improve the authenticity of the experiment, and the efficiency threshold of different GSI combinations under the combination modes can be studied.

5. Conclusions

In this study, we compared the results of 45 different GSI combinations in three different LCZ environments, highlighting the fundamental importance of LCZs and rainwater in evaluation. In recent years, high-temperature and heatwave conditions have gradually increased in China, resulting in frequent occurrences of extreme heat stress events. In Nanjing, for example, the population has increased by about 1.31 million people over the past decade, and the built-up area has increased by 174.3 km^2. The changes in urban form and population have changed the uses of landscapes and environments, making some surface materials, such as impervious surfaces and artificial lawns, more common. To develop urban construction in a more natural direction, it is necessary to propose infrastructure renovation according to the natural forms and meteorological conditions of the city. Therefore, the focus of this study was to examine the effects of modifying the thermal environment under the condition of afternoon rainfall during high-temperature heat waves in summer using materials with natural characteristics. Different combinations of measures achieve different levels of performance in terms of hydrothermal synergy, which are determined by the structure of the GSI itself and closely related to the solar radiation at the site, the air flow exchange between high and low spaces, and the shading effects of buildings and plants. The main conclusions of the study are as follows:

(1) The GSI combination is significantly related to the surface morphological characteristics of the study area. Among these, LCZ2, followed by LCZ1, most requires combinations of multiple forms of GSI to ensure that the GSI shows a strong cooling and humidification effect. In these two LCZs, it is necessary to ensure that there are both ground GSI (RG and PP) and facade GSI (VG and GR) in order to improve the

overall thermal comfort of the site. In LCZ3, a single GSI mode can also achieve a good effect in terms of improving thermal comfort, and this area is also the best area for improving thermal comfort using a combination of GSI modes. Among the four forms of GSI, VG has the best effect in terms of improving the thermal comfort of the site, followed by PP.

(2) Under conditions of high temperature and no rainfall, almost all mitigation measures are weakly effective at improving the thermal comfort of the outdoor environment. After rainfall, a more complex GSI combination leads to a cooling effect with a longer duration.

(3) In high-density urban neighborhoods, it is possible to achieve a comfortable outdoor environment only under the premise of providing shade in outdoor pedestrian recreation areas, then appropriately increasing the GSI of these areas. At the same time, increasing trees has a significant strengthening effect on the overall improvement effect.

The method proposed in this study can be used for systematic comparisons of the effects of different GSI combinations on outdoor thermal comfort in different LCZs and can be used for subsequent quantitative studies on the effects of GSI in subtropical environments.

Author Contributions: H.X.: conceptualization, methodology, software, investigation, formal analysis, and writing—review and editing. J.L.: investigation, software, formal analysis, writing—original draft, data curation, and visualization. Y.H.: writing—original draft, software, and data curation. All authors have read and agreed to the published version of the manuscript.

Funding: This work was supported by the Humanities and Social Science Fund of the Ministry of Education of the People's Republic of China (No. 20YJCZH190), the China Scholarship Council (No. 201808320046), and the Priority Academic Program Development of Jiangsu Higher Education Institutions (PAPD).

Data Availability Statement: The data that were used in this study are confidential.

Conflicts of Interest: The authors have no competing interests to declare that are relevant to the content of this article.

References

1. Oke, T.R.; Mills, G.; Christen, A.; Voogt, J.A. *Urban Climates*; Cambridge University Press: Cambridge, UK, 2017.
2. Souverijns, N.; De Ridder, K.; Veldeman, N.; Lefebre, F.; Kusambiza-Kiingi, F.; Memela, W.; Jones, N.K.W. Urban heat in Johannesburg and Ekurhuleni, South Africa: A meter-scale assessment and vulnerability analysis. *Urban Clim.* **2022**, *46*, 101331. [CrossRef] [PubMed]
3. Chapman, S.; Watson, J.E.M.; Salazar, A.; Thatcher, M.; McAlpine, C.A. The impact of urbanization and climate change on urban temperatures: A systematic review. *Landsc. Ecol.* **2017**, *32*, 1921–1935. [CrossRef]
4. Santamouris, M. Recent progress on urban overheating and heat island research. Integrated assessment of the energy, environmental, vulnerability and health impact. Synergies with the global climate change. *Energy Build.* **2020**, *207*, 109482. [CrossRef]
5. Xu, J.Y.; Dai, J.Y.; Wu, X.F.; Wu, S.Q.; Zhang, Y.; Wang, F.F.; Gao, A.; Tan, Y.P. Urban rainwater utilization: A review of management modes and harvesting systems. *Front. Environ. Sci.* **2023**, *11*, 1025665. [CrossRef]
6. Ding, F.; Pang, H.; Guo, W. Impact of the urban heat island on residents' energy consumption: A case study of Qingdao. *IOP Conf. Ser. Earth Environ. Sci.* **2018**, *121*, 032026. [CrossRef]
7. Jia, H.F.; Yao, H.R.; Tang, Y.; Yu, S.L.; Field, R.; Tafuri, A.N. LID-BMPs planning for urban runoff control and the case study in China. *J. Environ. Manag.* **2015**, *149*, 65–76. [CrossRef] [PubMed]
8. Cristan, R.; Aust, W.M.; Bolding, M.C.; Barrett, S.M.; Munsell, J.F.; Schilling, E. Effectiveness of forestry best management practices in the United States: Literature review. *For. Ecol. Manag.* **2016**, *360*, 133–151. [CrossRef]
9. Wong, T.H.F.; Chesterfield, C. *Water Sensitive Urban Design—A Stormwater Management Perspective*; Cooperative Research Centre for Catchment Hydrology and Melbourne Water Corporation: Melbourne, VIC, Australia, 2002.
10. Fletcher, T.D.; Shuster, W.; Hunt, W.F.; Ashley, R.; Butler, D.; Arthur, S.; Trowsdale, S.; Barraud, S.; Semadeni-Davies, A.; Bertrand-Krajewski, J.-L.; et al. SUDS, LID, BMPs, WSUD and more—The evolution and application of terminology surrounding urban drainage. *Urban Water J.* **2014**, *12*, 525–542. [CrossRef]
11. Roon, M.V.; Roon, H.V. *Low Impact Urban Design and Development: The Big Picture*; Manaaki Whenua Press: Lincoln, New Zealand, 2009.

12. Gong, C.; Hu, C.J. The research of gray space design of architecture based on green stormwater infrastructure application. In Proceedings of the International Conference—Alternative and Renewable Energy Quest (Areq 2017), Barcelona, Spain, 1–3 February 2017; pp. 219–228.
13. Afshari, A. A new model of urban cooling demand and heat island application to vertical greenery systems (VGS). *Energy Build.* **2017**, *157*, 204–217. [CrossRef]
14. Xia, T.; Zhao, B.; Yu, J.; Gao, Y.; Wang, X.; Mao, Y.; Zhang, J. Making residential green space exposure evaluation more accurate: A composite assessment framework that integrates objective and subjective indicators. *Urban For. Urban Green.* **2024**, *95*, 128290. [CrossRef]
15. Zhang, J.; Zhou, S.; Xia, T.; Yin, Y.; Wang, X.; Cheng, Y.; Mao, Y.; Zhao, B. Residential greenspace exposure, particularly green window-views, is associated with improved sleep quality among older adults: Evidence from a high-density city. *Build Environ.* **2024**, *253*, 111315. [CrossRef]
16. Coutts, A.M.; Tapper, N.J.; Beringer, J.; Loughnan, M.; Demuzere, M. Watering our cities: The capacity for Water Sensitive Urban Design to support urban cooling and improve human thermal comfort in the Australian context. *Prog. Phys. Geogr.* **2013**, *37*, 2–28. [CrossRef]
17. De Quadros, B.M.; Mizgier, M.G.O. Urban green infrastructures to improve pedestrian thermal comfort: A systematic review. *Urban For. Urban Green* **2023**, *88*, 128091. [CrossRef]
18. He, B.J.; Zhu, J.; Zhao, D.X.; Gou, Z.H.; Qi, J.D.; Wang, J.S. Co-benefits approach: Opportunities for implementing sponge city and urban heat island mitigation. *Land Use Policy* **2019**, *86*, 147–157. [CrossRef]
19. Palermo, S.A.; Turco, M. Green Wall systems: Where do we stand? In Proceedings of the Conference on Sustainability in the Built Environment for Climate Change Mitigation (SBE), Thessaloniki, Greece, 23–25 October 2019.
20. Pirouz, B.; Turco, M.; Palermo, S.A. A Novel Idea for Improving the Efficiency of Green Walls in Urban Environment—An Innovative Design and Technique. *Water* **2020**, *12*, 3524. [CrossRef]
21. Oquendo-Di Cosola, V.; Olivieri, F.; Ruiz-García, L. A systematic review of the impact of green walls on urban comfort: Temperature reduction and noise attenuation. *Renew. Sustain. Energy Rev.* **2022**, *162*, 112463. [CrossRef]
22. Tan, C.L.; Wong, N.H.; Jusuf, S.K. Effects of vertical greenery on mean radiant temperature in the tropical urban environment. *Landsc. Urban Plan.* **2014**, *127*, 52–64. [CrossRef]
23. Acero, J.A.; Koh, E.J.Y.; Li, X.X.; Ruefenacht, L.A.; Pignatta, G.; Norford, L.K. Thermal impact of the orientation and height of vertical greenery on pedestrians in a tropical area. *Build Simul.* **2019**, *12*, 973–984. [CrossRef]
24. Akbari, H.; Matthews, H.D. Global cooling updates: Reflective roofs and pavements. *Energy Build.* **2012**, *55*, 2–6. [CrossRef]
25. Besir, A.B.; Cuce, E. Green roofs and facades: A comprehensive review. *Renew. Sustain. Energy Rev.* **2018**, *82*, 915–939. [CrossRef]
26. An, K.J.; Lam, Y.F.; Hao, S.; Morakinyo, T.E.; Furumai, H. Multi-purpose rainwater harvesting for water resource recovery and the cooling effect. *Water Res.* **2015**, *86*, 116–121. [CrossRef] [PubMed]
27. Sadeghi, K.M.; Tam, W.; Kharaghani, S.; Loaiciga, H. University Park Neighborhood Rain Gardens Project in Los Angeles, California. In *World Environmental and Water Resources Congress 2019: Water, Wastewater, and Stormwater; Urban Water Resources; and Municipal Water Infrastructure, Proceedings of the World Environmental and Water Resources Congress 2019, Pittsburgh, PA, USA, 19–23 May 2019*; American Society of Civil Engineers: Reston, VA, USA, 2019; pp. 132–146.
28. Bruner, S.G.; Palmer, M.I.; Griffin, K.L.; Naeem, S. Planting design influences green infrastructure performance: Plant species identity and complementarity in rain gardens. *Ecol. Appl.* **2023**, *33*, e2902. [CrossRef] [PubMed]
29. Chapman, E.J.; Small, G.E.; Shrestha, P. Investigating potential hydrological ecosystem services in urban gardens through soil amendment experiments and hydrologic models. *Urban Ecosyst.* **2022**, *25*, 867–878. [CrossRef]
30. Kasprzyk, M.; Szpakowski, W.; Poznańska, E.; Boogaard, F.C.; Bobkowska, K.; Gajewska, M. Technical solutions and benefits of introducing rain gardens—Gdańsk case study. *Sci. Total Environ.* **2022**, *835*, 155487. [CrossRef]
31. Buzzard, V.; Gil-Loaiza, J.; Grachet, N.G.; Talkington, H.; Youngerman, C.; Tfaily, M.M.; Meredith, L.K. Green infrastructure influences soil health: Biological divergence one year after installation. *Sci. Total Environ.* **2021**, *801*, 149644. [CrossRef] [PubMed]
32. Burszta-Adamiak, E.; Biniak-Pieróg, M.; Dabek, P.B.; Sternik, A. Rain garden hydrological performance-Responses to real rainfall events. *Sci. Total Environ.* **2023**, *887*, 164153. [CrossRef] [PubMed]
33. Qin, Y.H. A review on the development of cool pavements to mitigate urban heat island effect. *Renew. Sustain. Energy Rev.* **2015**, *52*, 445–459. [CrossRef]
34. Seifeddine, K.; Amziane, S.; Toussaint, E.; Ouldboukhitine, S.E. Review on thermal behavior of cool pavements. *Urban Clim.* **2023**, *51*, 101667. [CrossRef]
35. Yang, J.Y.; Guo, Y.C.; Tam, V.W.Y.; Tan, J.J.; Shen, A.Q.; Zhang, J.F.; Zhang, C.; Lyu, Z. Research on pore-clogging behavior and mechanism in pervious concrete prepared with recycled aggregate. *Constr. Build. Mater.* **2023**, *384*, 131420. [CrossRef]
36. Kousis, I.; Pisello, A.L. Evaluating the performance of cool pavements for urban heat island mitigation under realistic conditions: A systematic review and meta-analysis. *Urban Clim.* **2023**, *49*, 101470. [CrossRef]
37. Wang, J.S.; Meng, Q.L.; Zou, Y.; Qi, Q.L.; Tan, K.H.; Santamouris, M.; He, B.J. Performance synergism of pervious pavement on stormwater management and urban heat island mitigation: A review of its benefits, key parameters, and co-benefits approach. *Water Res.* **2022**, *221*, 118755. [CrossRef]

38. Herath, H.M.P.I.K.; Halwatura, R.U.; Jayasinghe, G.Y. Modeling a Tropical Urban Context with Green Walls and Green Roofs as an Urban Heat Island Adaptation Strategy. In Proceedings of the 7th International Conference on Building Resilience: Using Scientific Knowledge to Inform Policy and Practice in Disaster Risk Reduction, Bangkok, Thailand, 27–29 November 2017; pp. 691–698.
39. Yang, X.; Yao, L.; Jin, T.; Jiang, Z. Temporal and spatial variations of local temperatures in the summer of Nanjing. *J. Civ. Environ. Eng.* **2019**, *41*, 160–167+174.
40. Schibuola, L.; Tambani, C. A monthly performance comparison of green infrastructures enhancing urban outdoor thermal comfort. *Energy Build.* **2022**, *273*, 112368. [CrossRef]
41. Fei, Z.; Tao, S.; Jian, W.; Jun, X.; Jinyi, L. Spatio-temporal Evolution Characteristics of Nanjing Heat Island Effect Based on Variation of Surface Parameters. *Remote Sens. Inf.* **2022**, *37*, 106–113.
42. Xu, H.; Sheng, K.; Zhang, M.; Zhang, J. Co-benefits balancing of low-impact development facilities on stormwater management and microclimate improvement on the high-rise residential area in Nanjing. *Urban Clim.* **2024**, *55*, 101904. [CrossRef]
43. Ouyang, W.L.; Morakinyo, T.E.; Ren, C.; Ng, E. The cooling efficiency of variable greenery coverage ratios in different urban densities: A study in a subtropical climate. *Build. Environ.* **2020**, *174*, 106772. [CrossRef]
44. Salata, F.; Golasi, L.; Petitti, D.; Vollaro, E.D.L.; Coppi, M.; Vollaro, A.D.L. Relating microclimate, human thermal comfort and health during heat waves: An analysis of heat island mitigation strategies through a case study in an urban outdoor environment. *Sustain. Cities Soc.* **2017**, *30*, 79–96. [CrossRef]
45. Giorio, M.; Paparella, R. Climate Mitigation Strategies: The Use of Cool Pavements. *Sustainability* **2023**, *15*, 7641. [CrossRef]
46. Faragallah, R.N.; Ragheb, R.A. Evaluation of thermal comfort and urban heat island through cool paving materials using ENVI-Met. *Ain Shams Eng. J.* **2022**, *13*, 101609. [CrossRef]
47. Liu, Z.X.; Cheng, W.W.; Jim, C.Y.; Morakinyo, T.E.; Shi, Y.; Ng, E. Heat mitigation benefits of urban green and blue infrastructures: A systematic review of modeling techniques, validation and scenario simulation in ENVI-met V4. *Build. Environ.* **2021**, *200*, 107939. [CrossRef]
48. Li, J.Y.; Zheng, B.H.; Chen, X.; Qi, Z.Y.; Bedra, K.B.; Zheng, J.A.; Li, Z.L.; Liu, L.Y. Study on a full-year improvement of indoor thermal comfort by different vertical greening patterns. *J. Build. Eng.* **2021**, *35*, 101969. [CrossRef]
49. Ren, J.Y.; Yang, J.; Zhang, Y.Q.; Xiao, X.M.; Li, X.M.; Wang, S.H.; Xia, J.C. Exploring thermal comfort of urban buildings based on local climate zones. *J. Clean. Prod.* **2022**, *340*, 130744. [CrossRef]
50. Morakinyo, T.E.; Ogungbenro, S.B.; Abolude, A.T.; Akinsanola, A.A. Quantifying the effect of rain events on outdoor thermal comfort in a high-density city, Hong Kong. *Int. J. Biometeorol.* **2019**, *63*, 19–27. [CrossRef] [PubMed]
51. Wang, Y.P.; Berardi, U.; Akbari, H. Comparing the effects of urban heat island mitigation strategies for Toronto, Canada. *Energy Build.* **2016**, *114*, 2–19. [CrossRef]
52. Lee, H.; Mayer, H.; Chen, L. Contribution of trees and grasslands to the mitigation of human heat stress in a residential district of Freiburg, Southwest Germany. *Landsc. Urban Plan.* **2016**, *148*, 37–50. [CrossRef]
53. Yang, X.S.; Zhao, L.H.; Bruse, M.; Meng, Q.L. Evaluation of a microclimate model for predicting the thermal behavior of different ground surfaces. *Build. Environ.* **2013**, *60*, 93–104. [CrossRef]
54. Ouyang, W.; Sinsel, T.; Simon, H.; Morakinyo, T.E.; Liu, H.; Ng, E. Evaluating the thermal-radiative performance of ENVI-met model for green infrastructure typologies: Experience from a subtropical climate. *Build. Environ.* **2022**, *207*, 108427. [CrossRef]
55. Chen, Y.; Zheng, B.; Hu, Y. Numerical Simulation of Local Climate Zone Cooling Achieved through Modification of Trees, Albedo and Green Roofs—A Case Study of Changsha, China. *Sustainability* **2020**, *12*, 2752. [CrossRef]
56. Detommaso, M.; Costanzo, V.; Nocera, F. Application of weather data morphing for calibration of urban ENVI-met microclimate models. Results and critical issues. *Urban Clim.* **2021**, *38*, 100895. [CrossRef]
57. Fabbri, K.; Costanzo, V. Drone-assisted infrared thermography for calibration of outdoor microclimate simulation models. *Sustain. Cities Soc.* **2020**, *52*, 101855. [CrossRef]
58. Galal, O.M.; Sailor, D.J.; Mahmoud, H. The impact of urban form on outdoor thermal comfort in hot arid environments during daylight hours, case study: New Aswan. *Build. Environ.* **2020**, *184*, 107222. [CrossRef]
59. Höppe, P. The physiological equivalent temperature—A universal index for the biometeorological assessment of the thermal environment. *Int. J. Biometeorol.* **1999**, *43*, 71–75. [CrossRef]
60. Walther, E.; Goestchel, Q. The P.E.T. comfort index: Questioning the model. *Build. Environ.* **2018**, *137*, 1–10. [CrossRef]
61. Qureshi, A.M.; Rachid, A.; Bartlett, D. Quantifying the cooling effect of urban heat stress interventions. *Int. J. Glob. Warm* **2023**, *30*, 60–80. [CrossRef]
62. Ouyang, W.L.; Morakinyo, T.E.; Lee, Y.L.; Tan, Z.; Ren, C.; Ng, E. How to quantify the cooling effects of green infrastructure strategies from a spatio-temporal perspective: Experience from a parametric study. *Landsc. Urban Plan.* **2023**, *237*, 104808. [CrossRef]
63. Mohajer, H.R.H.; Ding, L.; Santamouris, M. Developing Heat Mitigation Strategies in the Urban Environment of Sydney, Australia. *Buildings* **2022**, *12*, 903. [CrossRef]
64. Wong, N.H.; Tan, C.L.; Kolokotsa, D.D.; Takebayashi, H. Greenery as a mitigation and adaptation strategy to urban heat. *Nat. Rev. Earth Environ.* **2021**, *2*, 166–181. [CrossRef]
65. Krebs, L.F.; Johansson, E. Influence of microclimate on the effect of green roofs in Southern Brazil—A study coupling outdoor and indoor thermal simulations. *Energy Build.* **2021**, *241*, 110963. [CrossRef]

66. Mutani, G.; Todeschi, V. The Effects of Green Roofs on Outdoor Thermal Comfort, Urban Heat Island Mitigation and Energy Savings. *Atmosphere* **2020**, *11*, 123. [CrossRef]
67. Norton, B.A.; Coutts, A.M.; Livesley, S.J.; Harris, R.J.; Hunter, A.M.; Williams, N.S.G. Planning for cooler cities: A framework to prioritise green infrastructure to mitigate high temperatures in urban landscapes. *Landsc. Urban Plan.* **2015**, *134*, 127–138. [CrossRef]
68. Li, Z.L.; Chow, D.H.C.; Yao, J.; Zheng, X.; Zhao, W. The effectiveness of adding horizontal greening and vertical greening to courtyard areas of existing buildings in the hot summer cold winter region of China: A case study for Ningbo. *Energy Build.* **2019**, *196*, 227–239. [CrossRef]
69. Xu, H.; Zhong, T.; Chen, Y.; Zhang, J. How to simulate future scenarios of urban stormwater management? A novel framework coupling climate change, urbanization, and green stormwater infrastructure development. *Sci. Total Environ.* **2023**, *874*, 162399. [CrossRef] [PubMed]
70. Saraswat, C.; Kumar, P.; Mishra, B.K. Assessment of stormwater runoff management practices and governance under climate change and urbanization: An analysis of Bangkok, Hanoi and Tokyo. *Environ. Sci. Policy* **2016**, *64*, 101–117. [CrossRef]
71. Peng, L.L.H.; Jiang, Z.D.; Yang, X.S.; He, Y.F.; Xu, T.J.; Chen, S.S. Cooling effects of block-scale facade greening and their relationship with urban form. *Build. Environ.* **2020**, *169*, 106552. [CrossRef]
72. Zheng, X.; Hu, W.; Luo, S.; Zhu, Z.; Bai, Y.; Wang, W.; Pan, L. Effects of vertical greenery systems on the spatiotemporal thermal environment in street canyons with different aspect ratios: A scaled experiment study. *Sci. Total Environ.* **2023**, *859*, 160408. [CrossRef]
73. Jin, C.; Bai, X.; Luo, T.; Zou, M. Effects of green roofs' variations on the regional thermal environment using measurements and simulations in Chongqing, China. *Urban For. Urban Green.* **2018**, *29*, 223–237. [CrossRef]
74. Liu, A.W.; Ma, X.Y.; Du, M.; Su, M.F.; Hong, B. The cooling intensity of green infrastructure in local climate zones: A comparative study in China's cold region. *Urban Clim.* **2023**, *51*, 101631. [CrossRef]
75. Peng, L.L.H.; Jim, C.Y. Green-Roof Effects on Neighborhood Microclimate and Human Thermal Sensation. *Energies* **2013**, *6*, 598–618. [CrossRef]
76. Priya, U.K.; Senthil, R. A review of the impact of the green landscape interventions on the urban microclimate of tropical areas. *Build. Environ.* **2021**, *205*, 108190. [CrossRef]
77. Sandoval, G.F.B.; Pieralisi, R.; Risson, K.D.B.D.; de Moura, A.C.; Toralles, B.M. Clogging phenomenon in Pervious Concrete (PC): A systematic literature review. *J. Clean Prod.* **2022**, *365*, 132579. [CrossRef]
78. Li, H.; Harvey, J.; Jones, D. Cooling Effect of Permeable Asphalt Pavement Under Dry and Wet Conditions. *Transp. Res. Rec.* **2013**, *2372*, 97–107. [CrossRef]
79. Teichmann, F.; Horvath, A.; Luisser, M.; Korjenic, A. The Impact of Small-Scale Greening on the Local Microclimate—A Case Study at Two School Buildings in Vienna. *Sustainability* **2022**, *14*, 13089. [CrossRef]